Geophys. J. Int. (2006) **166,** 767–781 doi: 10.1111/j.1365-246X.2006.03036.x

Deep origin of the Hawaiian tilted plume conduit derived from receiver functions

I. Wölbern,[1,*] A. W. B. Jacob,[2,†] T. A. Blake,[2] R. Kind[1,‡] X. Li,[1] X. Yuan,[1] F. Duennebier[3] and M. Weber[1,§]

[1] *GeoForschungsZentrum Potsdam, Telegrafenberg,* 14473 *Potsdam, Germany*
[2] *Dublin Institute for Advanced Studies,* 5 *Merrion Square, Dublin* 2, *Ireland*
[3] *School of Ocean & Earth Science & Technology, University of Hawaii, Honolulu, HI, USA*

Accepted 2006 April 11. Received 2006 April 4; in original form 2005 May 6

SUMMARY

We employ *P* to *S* converted waveforms to investigate effects of the hot mantle plume on seismic discontinuities of the crust and upper mantle. We observe the Moho at depths between 13 and 17 km, regionally covered by a strong shallow intracrustal converted phase. Coherent phases on the transverse component indicate either dipping interfaces, 3-D heterogeneities or lower crustal anisotropy. We find anomalies related to discontinuities in the upper mantle down to the transition zone evidently related to the hot mantle plume. Lithospheric thinning is confirmed in greater detail than previously reported by Li *et al.*, and we determine the dimensions of the low-velocity zone within the asthenosphere with greater accuracy. Our study mainly focuses on the temperature-pressure dependent discontinuities of the upper mantle transition zone. Effects of the hot diapir on the depths of mineral phase transitions are verified at both major interfaces at 410 and 660 km. We determine a plume radius of about 200 km at the 660 km discontinuity with a core zone of about 120 km radius. The plume conduit is located southwest of Big Island. A conduit tilted in the northeast direction is required in the upper mantle to explain the observations. The determined positions of deflections of the discontinuities support the hypothesis of decoupled upper and lower mantle convection.

Key words: convection, Hawaii, hotspots, mantle discontinuities, mantle plume, receiver functions.

1 INTRODUCTION

Hawaii is the most prominent example of intraplate volcanism linked to a linear island chain. Increasing age of the volcanic islands in conjunction with chemical differences between ocean island and mid-ocean-ridge basalts resulted in the concept of mantle plumes (Wilson 1963; Morgan 1971). Today, the theory of mantle plumes, as an important part of the mantle convecting system, is widely accepted, but some aspects are still unresolved. Several papers report varying numbers of hotspots worldwide (e.g. Morgan 1971; Seidler *et al.* 1999; Steinberger 2000). So far, only a couple of mantle plumes are clearly related to upper mantle anomalies, for example, Iceland (Shen *et al.* 1998), Yellowstone (Fee & Dueker 2004), Eifel (Budweg *et al.* 2006), Massif Central (Sobolev *et al.* 1997), and only a few diapirs clearly extend into the lower mantle (e.g. Ritsema & Allen 2003; Montelli *et al.* 2004).

Mantle diapirs originate from instabilities at a thermal boundary layer. The D″ layer situated at the core–mantle boundary has for a long time been thought to be the sole possible origin of mantle plumes. Another possible thermal boundary layer is proposed underneath the 660 km discontinuity, as its endothermic phase change acts as a barrier to vertical flow and, thus, can retard or even stop ascending volumes (Cserepes & Yuen 2000; Cserepes *et al.* 2000; Marquart & Schmeling 2000). Transition zone thickness is a helpful tool to detect mantle plumes, because mineral transitions at depths of 410 and 660 km have contrary responses in relation to pressure and temperature (e.g. Bina & Helffrich 1994). Hot mantle plumes ascending to the upper mantle, accordingly, will reduce the thickness of the mantle transition zone (MTZ) by lowering the 410 km discontinuity and elevating the 660 km discontinuity. The horizontal extent of the updoming area of the 660 gives information about the depth of origin (Shen *et al.* 1998). A comparative study reveals that variations on transition zone thickness at most oceanic hotspot sites do not show significant differences from bulk oceanic mantle.

*Now at: J. W.-Goethe Universität, Frankfurt, Germany. E-mail: woelbern@geophysik.uni-frankfurt.de
†Prof A. W. Brian Jacob died on 2001 November 5. It was a great honour for us to have worked with him and we appreciate his committment in the face of poor health.
‡Also at: Freie Universität Berlin, Malteserstr. 74-100, 12249 Berlin, Germany.
§Also at: Universität Potsdam, Potsdam, Germany.

Only a few hotspots are linked to noticeable thinning of the transition zone (Li *et al.* 2003a,b). However, data are each provided from single stations, covering only zonular regions limited to a minimum distance of approximately 80 km from the station location at depth of 410 km. A network of seismic stations, as it is used in this study, is required to sufficiently sample the entire target area.

The plume source is generally assumed to be fixed relative to the moving lithosphere. However, a slight drift of the source by about 1–2 mm yr^{-1} is expected from laboratory experiments (Davaille *et al.* 2002). Different authors reason considerably higher drift velocities at the surface (e.g. Wang & Wang 2001; Tarduno *et al.* 2003; McNamara & Zhong 2004; Steinberger *et al.* 2004). Furthermore, the 43-Myr-old bend in the Hawaii-Emperor chain is proposed to be caused by a change of motion of the Hawaiian plume itself rather than a change of plate direction (Norton 1995; Tarduno & Cotrell 1997; Tarduno *et al.* 2003). In a viscous mantle it is likely that mantle diapirs are sidetracked by convective flow. Changes of convective flow pattern would affect the orientation of the plume conduit resulting in hotspot motion at the surface even when the plume source is stationary (Wang & Wang 2001; Stock 2003; Tarduno *et al.* 2003; Steinberger *et al.* 2004). Thus, the lateral position of the plume conduit at different depths provides conclusions about the nature of mantle convection.

So far, neither the source location nor the orientation of the Hawaiian plume conduit are well determined. Tomography studies reveal anomalies beneath the Hawaiian hotspot (Zhao 2001; Montelli *et al.* 2004), but there is no clear evidence for a lower mantle source. An analysis of core reflected waves exhibited strong anisotropy interpreted as the plume source region at the D″ layer (Russel *et al.* 1998; Fouch *et al.* 2001), however, the derived lateral positions diverge a lot. Gaherty *et al.* (1996) propose thinning of the transition zone between Hawaii-Tonga in the velocity model PA5. Derived from receiver function analysis a confined area of updoming of the 660 km discontinuity is located southwest of the Big Island (Li *et al.* 2000) possibly extending several hundred km along the southern side of the Hawaiian swell (Collins *et al.* 2002). Both studies, however, are based on small data sets providing very sparse lateral coverage not allowing for exact localization. Using a much denser data base, in this study we map in greater detail effects of the mantle plume on discontinuities and structures from the crust down to the uppermost lower mantle underneath Hawaii.

2 DATA AND METHOD

The Hawaii plume project was carried out by the Dublin Institute of Advanced Studies (DIAS, Ireland) in cooperation with the GeoForschungsZentrum (GFZ, Potsdam, Germany) and the School of Ocean & Earth Science & Technology (SOEST, Honolulu, Hawaii). Starting in 1999 June a set of 11 mobile broad-band seismic instruments was installed by DIAS in assistance from SOEST, University of Hawaii. Instruments were distributed over the four biggest of the Hawaiian islands with concentration on the Big Island. Stations were equipped with Guralp-40T seismometers using EDL digital recorders with sampling frequencies of 25 and 75 Hz, respectively. The temporary array was continuously recording data until their removal in 2001 May. GEOFON station MAUI was set up by the GFZ also in 1999 June. MAUI is equipped with a Streckeisen STS-2 broad-band instrument and a RefTek digital data logger recording with 20 Hz sampling frequency. Additional data was used from IRIS-/USGS network permanent stations POHA on Big Island and GEOSCOPE station KIP on Oahu. We use also recordings from a few events from temporary stations KHU, STC, UXL and broadband array HIBSN operated by the USGS on Big Island and from the permanent IRIS-/USGS station MIDW on Midway. A total of 19 stations contributes to our study, distribution of which is shown in Fig. 1.

In order to examine *P* to *S* converted phases we choose teleseismic earthquake recordings with epicentral distances between 35° and 95°. We select events of magnitude 5.7 and greater at each station for the time period of the Hawaii plume project. The epicentral distribution of these events is shown in Fig. 2. The best coverage

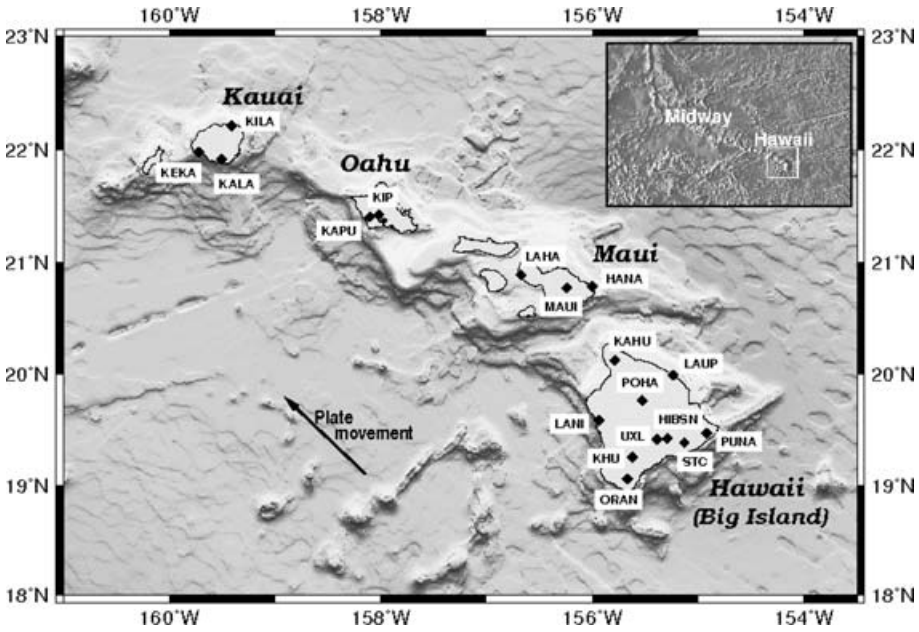

Figure 1. Locations of temporary and permanent stations used in this study. Seismometers are distributed over the four biggest of the Hawaiian islands concentrated on the Big Island. Additional recordings are used from station Midway (see text for further details).

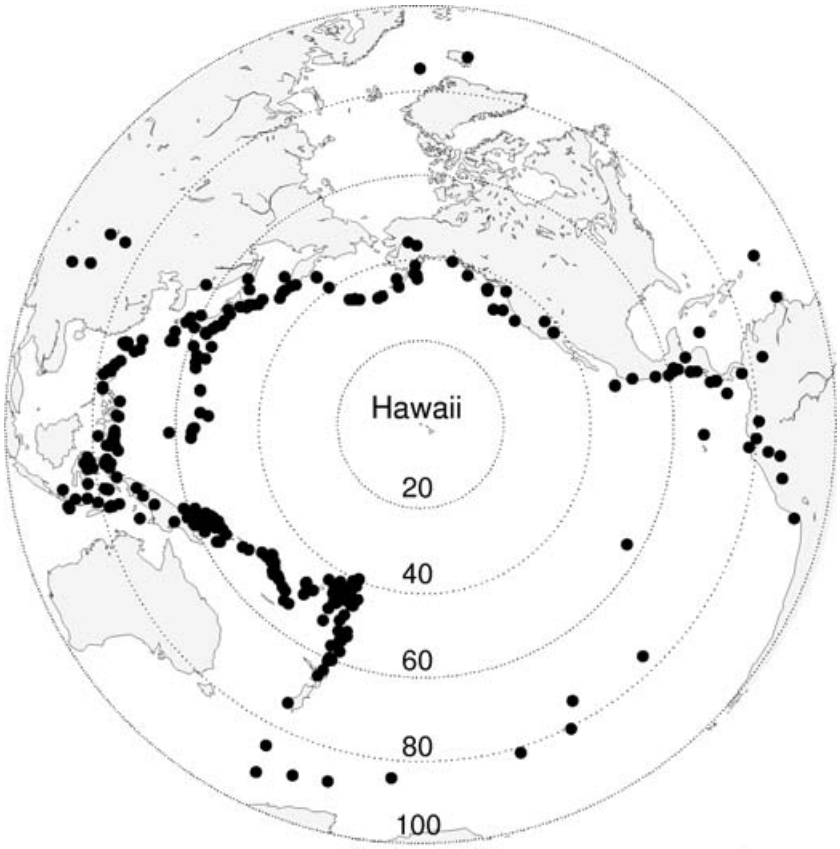

Figure 2. Distribution of teleseismic earthquakes during the operational period of the temporary network. Circles indicate distances given in degrees. Best azimuthal coverage is obtained in southwest to northern directions.

is obtained in the backazimuthal ranges of 80° to 100° and 200° to 360°. On Oahu, permanent station KIP has been operational for several years. Here, we extend the data set by supplementary events of magnitude 6.5 and greater beginning 1988 October.

First, traces are resampled with 20 Hz. We apply a displacement restitution filter to restore true ground motion. Receiver functions are computed following the procedure described by Yuan *et al.* (1997). We rotate three-component seismograms into the ray coordinate system (*L*, *Q*, *T*) oriented in directions of *P*-, *SV* and *SH* waves, respectively. We determine the rotation angles (backazimuth and incidence angle) by the eigenvalues of the covariance matrix from the observed *P* wave. Also, theoretical angles are computed on the basis of hypocenters and station locations using the IASP91 reference model (Kennett & Engdahl 1991) and we calculate the differences of both. We use observed angles for deviations up to 40° and 30° in backazimuth and incidence angle, respectively, or else theoretical angles are taken, to avoid false observed angles caused by noise effects. If the deviation of the incidence angle exceeds 50°, we remove the event has been removed from the data set. In order to reduce the noise level we derive eigenvalues from filtered seismograms. Final receiver functions are computed by deconvolving *P* waveforms on the *L*-component from the corresponding *Q*- and *T*-components. We obtain a total of 1923 receiver functions.

In order to increase the signal-to-noise ratio we stack receiver functions from different earthquakes. Summation enhances coherent phases while random background noise is suppressed. The delay time of a converted phase at given depth relative to the originating *P* wave changes with epicentral distance. Therefore, we apply a moveout correction before stacking. We use a reference slowness of 6.4 s/° corresponding to an epicentral distance of 67°. The bootstrap method (Efron & Tibshirani 1986) is applied to check for stability of coherent signal: From the traces in a selected area we randomly choose subsets of about half the original number. Subsets are stacked and compared. We expect converted phases to occur in all subsets while non-seismic signal should affect only a few of them. Simultaneously, the range of depth of a discontinuity can be derived from varying arrival times in different subsets.

3 RESULTS

3.1 Crustal structure

We examine the crustal thickness along the island chain. The piercing points related to the crust-mantle boundary are distributed over a region of about 3 km radius around each station. By stacking we derive a mean depth to the Moho at each location. In a first step a bandpass filter from 1 to 30 s is used. The summed traces have revealed strong conversions with delay times systematically decreasing towards the southeast (like apparent in Fig. 5; see below). Resulting depths to Moho are clearly unrealistic. To increase resolution we enhance the short-period portion of the signal by applying a WWSSN-SP simulation filter (McCowan & La Coss 1978) to the restituted data. We use an additional bandpass filter from 0.25 to 3 Hz to suppress high frequency oceanic noise. Fig. 3 shows the first 10 s of the resulting summed traces sorted by station locations along a profile defined by the island chain. Two phases followed by multiples can be discriminated within the first 2 s at most

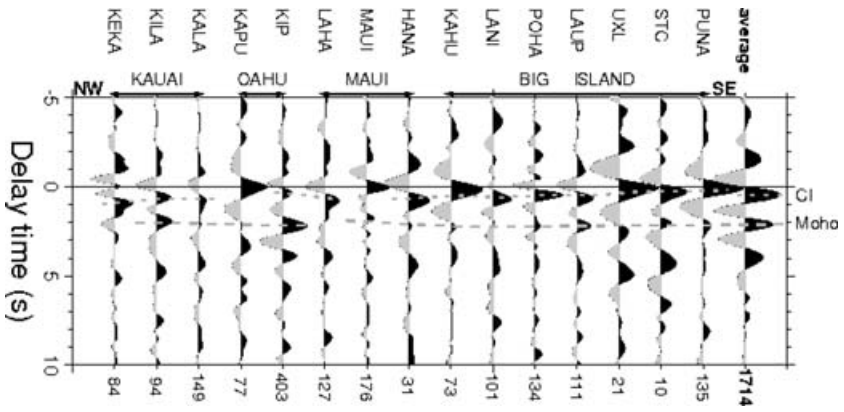

Figure 3. Sum traces from single stations along the island chain from Kauai (left) to the Big Island (right). A short-period simulation filter (WWSSN-SP) is applied after restitution. In a second step data are bandpass filtered with a passband of 0.25–3 Hz and receiver functions are stacked. The numbers of traces used in every stack are given at the bottom of each trace. The rightmost trace shows the average in the area under investigation. The biggest amplitudes at most stations occur within the first few second after the *P* onset (marked as CI). Multiples from these strong conversions partially interfere with later arrivals. However, Moho phases can be identified in most traces (marked Moho). Arrival times are roughly ranging from 1.8 to 2.2 s. Later phases in the section relate to crustal multiples.

stations, the first of which ranges between nearly 0 and 0.8 s, and is assumed to originate at an intracrustal interface (marked and hereafter referred to as CI). The time corresponds to depths of max. 6 km below sea level, which is obviously too shallow for the Moho. The CI phase seems to alter systematically. In general, from NW to SE the delay times relative to *P* onset decrease, while amplitudes increase compared to Moho. This may be coincidental. As a first model, we infer a dipping structure with increasing velocity contrast towards the recent volcanism (SE). However, there is no evidence for a continuous CI phase along the island profile, because ray paths at that depths do not overlap. The nature of the velocity change remains unclear, but it can reasonably be linked to volcanic causes. The very strong positive phases in the SE could originate at the bottom of a magma chamber, as being supposed beneath Kilauea at 2 to 4 km depth (Pietruszka & Garcia 1999). Subsidence combined with cooling might be a plausible explanation for both, the observed deepening and impedance decrease towards NW. Wang *et al.* (2003) suggest the addition of a low-δ^{18}O component to the magmas which are parental to cored HSDP-2 lavas on Big Island. They focus on two models involving contamination in the lithosphere or volcanic edifice. One of which is the 'MASH'-zone model (Melting-Assimilation-Storage-Homogenization) assuming partial melting within the crust as source of the low-δ^{18}O component: Melting is supposed to be caused by repeated intrusion of magma producing a complex of dikes and sills, which could also generate strong conversions variable in depth and decreasing in velocity contrast as the magma cools and solidifies. However, we have to point out the rather low signal-to-noise ratio at some of the stations.

The second phase in Fig. 3 (dashed line, labelled as Moho) relates to the crust-mantle boundary. It is difficult to detect at many stations due to the interfering crustal phase (CI) and reverberations in the crust. We deduce depths to Moho from Fig. 3. The theoretical depth resolution of the receiver functions is about 1 km, but noise and interference with crustal multiples would increase this value. The interferences provoke a time-shift of the detected amplitude maxima inducing incorrect readings. Beneath Kauai we obtain values of 15 to 16 km from stations KALA and KILA while at KEKA the Moho phase seems to be completely suppressed. The depth increases to about 17 km beneath the island of Oahu. This is in good agreement with previous results (Lindwall 1988). At the island of Maui we achieve increasing values to the southeast with a mean depth to Moho of about 13 km. However, results at stations LAHA and HANA are not convincing, as the noise level is rather high. Underneath the Big Island the Moho depth is between 15 and 17 km, which is up to 5 km more than reported in previous studies (e.g. Crosson & Koyanagi 1979; Zucca & Hill 1980). The comparative weakness of the Moho conversion can be explained as follows: (1) The velocity contrast is considerably higher at the CI (potentially the contact between the oceanic basaltic layer 2 and the gabbroic layer 3) than at the Moho. This is not unlikely since the oceanic Moho exhibits a rather small velocity change, particularly with regard to hot volcanic material remaining at the Moho. James & Savage (1990) also report complex waveforms of Moho reflections beneath Big Island contradicting a simple Moho structure. (2) If the CI is strong, it will also cause pronounced multiples, thus the Moho signal might be masked by interfering multiple phases. (3) Delay times of the summed traces could vary within the lateral window due to the topography of the interface or azimuthal dependence of seismic velocity. Phases can, therefore, not be stacked coherently and the signal becomes smeared out or even annihilated.

We also find distinct coherent phases on the transverse component (*T*-component). Fig. 4 presents representative sections of *Q*- and *T*-components at the permanent station KIP. This example illustrates the variation of receiver functions with backazimuth. All traces are equally spaced, and the corresponding backazimuths are indicated. The best coverage is accomplished in the sectors from 80° to 100° and 200° to 350° as expected from seismicity (see Fig. 2). The Moho stands out clearly on the *Q*-component (Fig. 4a). A rigorous change of arrivals can be noticed at KIP in the eastern azimuthal range indicating complex structures within the crust. We also find a number of coherent phases on the *T*-component (Fig 4b), that is, energy is projected off the incident plane onto the transverse component. Such may originate, for example, from anisotropic layers, dipping interfaces or 3-D heterogeneities, usually showing systematic polarity changes (Jones & Phinney 1998). At KIP the azimuthal coverage is sufficient to reliably determine a periodicity of 360° with polarity changing at backazimuths of 300° and *ca.* 120°. We detect latest Moho arrivals at backazimuth of 300°, which would relate to the downdip direction in the case of a dipping interface. Depths to

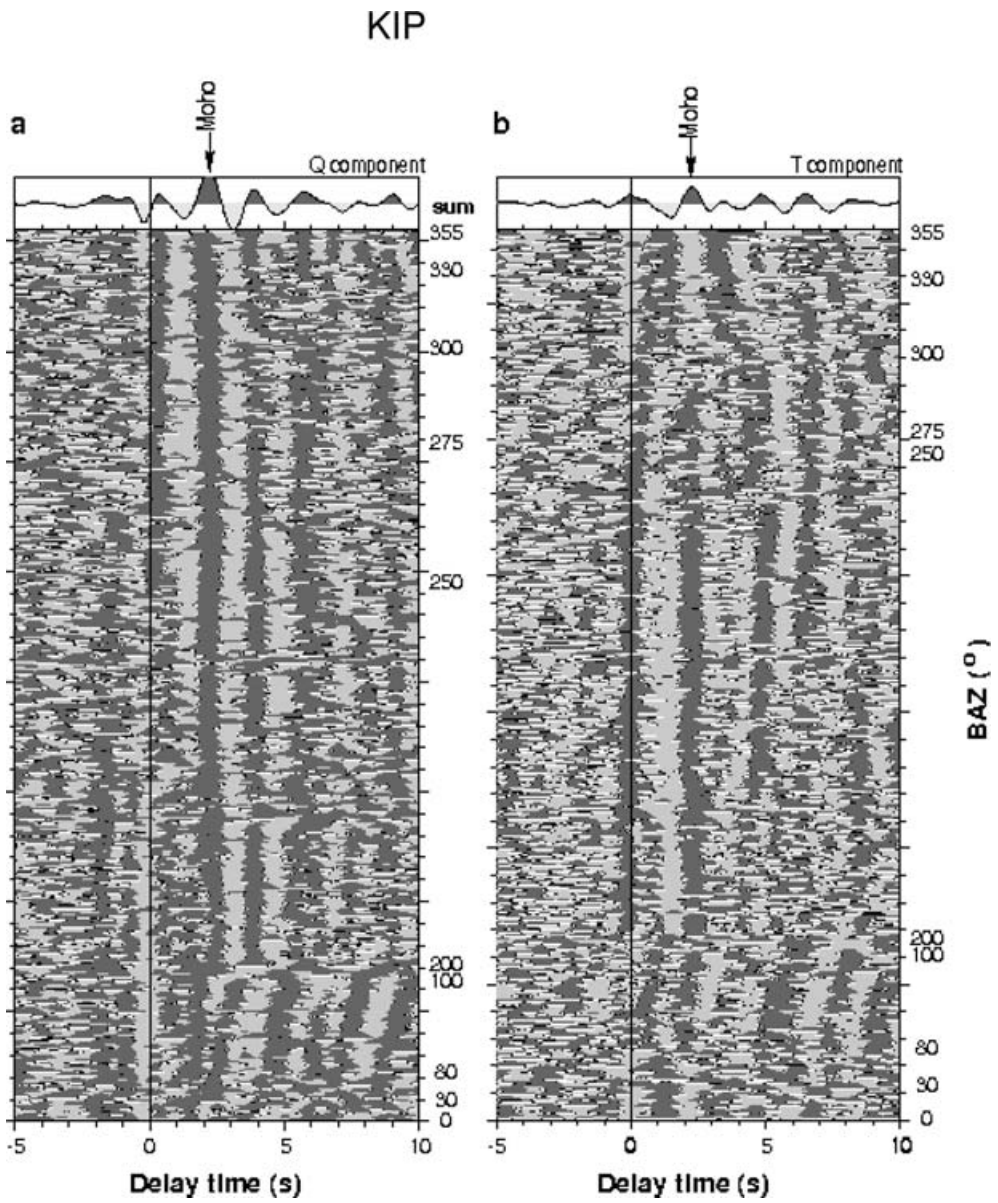

Figure 4. Time section of single receiver functions recorded at station KIP on Oahu. We use filters as described in Fig. 3. Traces are equally spaced and sorted by backazimuth (see labels at right). (a) *Q*-component: The Moho is detected as the most prominent structure followed by multiples. Waveforms drastically differ from northern to eastern azimuths (left) indicating varying structure beneath the station. (b) *T*-component: Pronounced coherent phases occur at Moho time and even earlier. The polarity is changing with a periodicity of 360°.

Moho have been determined to be 17 and 15 km in the downdip and updip direction, respectively. This corresponds to a dip angle of about 20°, which would also apply to the phase occurring about half a second earlier. Yet, the observation could also be explained by an anisotropic layer with a non-horizontal symmetry axis which is difficult to distinguish from a dipping interface as discussed in Savage (1998). We compute synthetic seismograms (not shown) using the reflectivity code written by Levin & Park (1997). A model comprising a layer with about 10 per cent anisotropy roughly between 12 and 17 km depth, that is, the oceanic crust underneath the volcanic edifice, best matches the observations. Polarity changes, in this case, indicate a symmetry axis oriented parallel to the island chain with a dip angle of about 45° and the updip direction at a backazimuth of 300°. However, complex volcanic structures are suggested above in the context of the crustal interface. Thus, local heterogeneities must be considered, which could also be responsible or contribute to the observed phases.

3.2 Thickness of the lithosphere

The lithosphere–asthenosphere boundary (hereafter referred to as LAB) is generally believed to be an isotherm near the solidus. While the oceanic plate cools with age the lithosphere progressively thickens. For an oceanic plate 90 to 100 million years old such as around Hawaii a lithospheric thickness of about 90 km is expected (Detrick & Crough 1978). This value is in general agreement with previous studies (e.g. Bock 1991; Laske *et al.* 1999; Priestley & Tilmann 1999). Recently, changes of lithospheric thickness have been discovered by means of *S*-receiver functions compared with results from *P*-receiver functions at the stations KIP, MAUI and POHA.

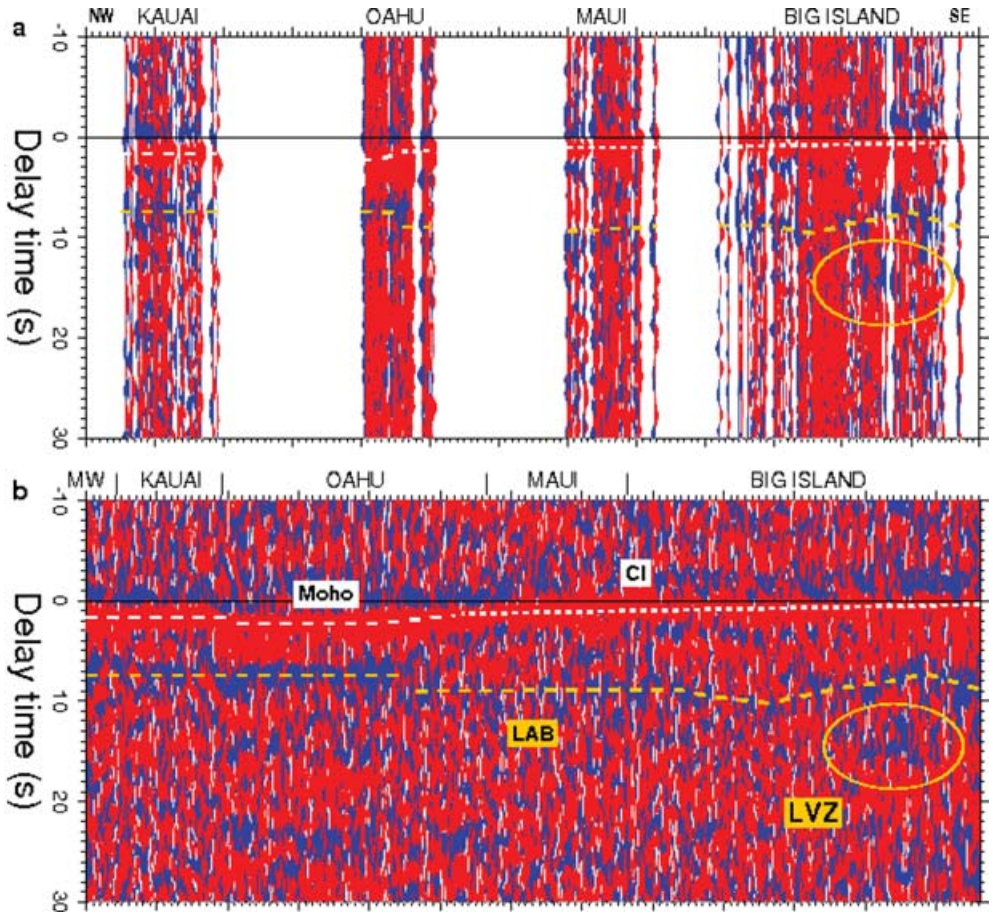

Figure 5. Section of single receiver functions sorted along the island profile. A bandpass filter from 2 to 30 s is applied. Traces are displayed in order of piercing points calculated for a depth of 100 km from NW to the Big Island (from left to right). In (a) receiver functions are collocated in real distance mapping the actual structures. (b) Traces are equally spaced. Here, also data from station MIDW at far (left) are incorporated. Most prominent conversions are labelled. The first arrival is generated at a structure which seemingly shallows towards SE. This is the result of the Moho conversion merged with the signal from the crustal interface shown in Fig. 3. The two phases cannot be separated at the frequencies used. Shallow conversions dominate in the southeast (CI), while the Moho signal is stronger in the NW. The negative signal termed LAB is interpreted as Gutenberg discontinuity. It is more perspicuous from Oahu to the NW where it also occurs a little earlier. Below Big Island the LAB seems to be first deflected downward, then deflected upward at the same place where an additional negative phase can be seen, labelled LVZ.

Gradual thinning of the lithosphere from 100 to 110 km under Big Island to about 50 to 60 km below Kauai is revealed directly beneath the island chain in a corridor with a width of about 300 km (Li *et al.* 2004).

We significantly enlarge the data set by including the entire temporary network described above and analyse in greater detail the LAB below Hawaii. In Fig. 5 a total of 630 single receiver functions is sorted by piercing points at 100 km depth along the island profile. Positive velocity contrasts (i.e. increasing velocity with increasing depth) are displayed in red and negative contrasts are shown in blue. In the upper section (Fig. 5a) traces are displayed at their real distance along the island chain. In the section below (Fig. 5b) traces are equally spaced and a few receiver functions obtained at stations MIDW are added (see Fig. 1 for station location). We mark three features: (1) the crustal phase (CI) merging into the Moho phase beneath Oahu and Kauai, (2) a negative phase assumedly representing the LAB and (3) a local negative anomaly situated below the LAB underneath Big Island, that we further discuss in Section 3.3. A bandpass filter from 2 to 30 s is applied, so the phases generated at CI and at the Moho cannot be discriminated. Early CI arrivals dominate the section from SE-Oahu to Big Island (white short-dashed line), while the Moho signal (white long-dashed line) becomes stronger towards the NW.

The pronounced negative phase at about 8 to 10 s (Fig. 5, dashed yellow line) we relate to the LAB. Delay time relative to *P* onset is decreasing along the profile from SE to NW confirming the results of the *S*-receiver functions (Li *et al.* 2004). However, crustal multiples are expected to interfere with the LAB phase. By computing inversion models we verify the influences of crustal interfaces at station KIP (Fig. 6) starting with a simplified model from Lindwall (1988). First, we invert for a velocity model containing crustal interfaces only. From the resulting model (Fig. 6 left, thin line) a synthetic receiver function (Fig. 6 right, thin trace) is obtained. This satisfactorily explains the first 10 s of the observed trace (dashed line), but fails to reproduce the succeeding negative phase at approximately 24 s. The late negative arrival (blue) can also be traced along the profile in Fig. 5 at approximately the same time. In a second velocity model we add the LAB discontinuity at 60 km depth. The final model is given by the thick line in Fig. 5 (left). We compare again the resulting theoretical receiver function (Fig 8, right bottom, thick trace) with the data (dashed line). Including the LAB interface improves the fit of the first 9 s. We infer that, both, crustal

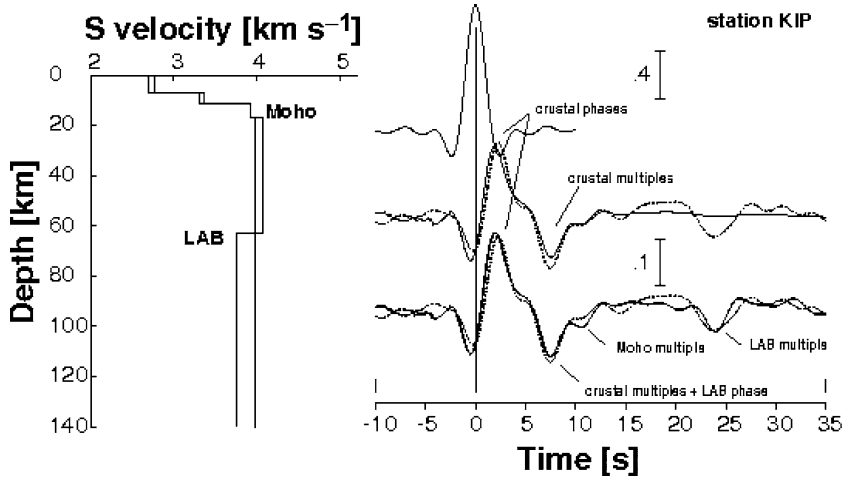

Figure 6. Comparison of velocity structures acquired by inversion of averaged receiver functions at station KIP. The dashed traces on the right show the *Q*-component of the data. The corresponding *L*-component is displayed on top. The thin line on the left denotes a simple model without LAB. The resulting *Q*-component is the thin line (right, middle): The first 10 s match well with the data. A later, negative arrival at about 25 s, however, cannot be explained as a crustal multiple. This phase can only be modelled by adding a further interface (LAB) like shown in the second model (left, thick line).

multiples and a direct phase generated at the LAB contribute to this negative phase occurring at *ca.* 7.5 s at station KIP, also explaining the strong amplitude observed. As the velocity contrast at the Moho is increased in the final model, now a weak negative multiple phase (*PpSs & PsPs*) occurs following at roughly 10 s. The existence of a strong LAB is confirmed by the negative signal at 24 s modelled as a multiple phase. We rule out the case of a direct converted phase at 24 s, which, according to IASP91 (Kennett & Engdahl 1991), would require a low-velocity zone (LVZ) at a depth of *ca.* 220 km where the Lehmann discontinuity would rather be expected. Also, we do not observe any multiples related to such a discontinuity.

According to IASP91 (Kennett & Engdahl 1991) we derive lithospheric thicknesses from approximately 90 km beneath Big Island decreasing towards NW to about 65 km underneath Oahu. Beneath Big Island the LAB exhibits a local anomaly. This anomaly coincides with an additional phase at about 14 s (marked as LVZ in Fig. 5b) discussed in Section 3.3. Here, the LAB phase occurs about 2 s earlier, and it also appears weaker compared to other traces recorded at Big Island (see also Figs 7a and b). Influences on the LAB by sidelobes related to the later phase can be excluded by applying more short-period filters (not shown). The origin of the early phase is ambiguous. If it corresponds to the LAB, this would indicate a sharply terminated area of lithospheric thinning by about 15 to 20 km potentially caused by the excess temperature of the impinging plume conduit. However, the arrival time of about 7 s is also in accord with theoretical arrivals of negative multiples corresponding to Moho or CI. Thus, it is possible that the LAB is seismically invisible in this region due to melting processes which generate a large zone of gradually changing velocities. None of these settings can be completely ruled out until further modelling has been accomplished (S.V. Sobolev, personal communication, 2005).

The depth to the LAB obtained from this study slightly differs from the results from *S*-receiver functions, something already noted and discussed by Li *et al.* (2004). However, there is good agreement in the general tendency from age consistent, normal oceanic lithosphere in the area of Big Island to distinctive thinning beneath Oahu and further NW. This is explained by thermal plume-lithosphere interaction: The lithosphere is heated from below by plume material dragged off by the overriding plate, thus, forming a tail-like channel along the island chain (Li *et al.* 2004; Ribe 2004). The thinnest lithosphere is found after 3–4 Myr beneath Oahu, and thickness remains constant towards Kauai. Following this model, the lithosphere is supposed to thicken again as the plume material cools down. We compute additional data recorded at station MIDW on the island of Midway, about 2000 km NW of our study area (see Fig. 1). The *P*-receiver functions reveal a depth to LAB of about 65 km comparable to results obtained for Kauai (Fig. 5b), indicating that the lithosphere is still thinned. In contrast, *S*-receiver functions at MIDW indicate a depth to LAB of about 100 km which has also been reported in previous studies with to Rayleigh waves (Woods *et al.* 1991; Woods & Okal 1996). This discrepancy we explain by the different areas sampled by the two methods: the piercing points of the *P* receiver functions are located at about 30 km distance around the station whereas the piercing points corresponding to *S*-receiver functions are located further away at approximately 120 km. We suggest, that cooling of the plume material has narrowed the channel of thinned lithosphere, but rethickening is not completed. However, this is rather speculative because we have only investigated a small number of receiver functions not allowing for a detailed image of the seismic structure. For reliable conclusions detailed investigation of further data at MIDW is mandatory.

3.3 Low-velocity zone

Beneath the central part of Big Island a negative phase is reported below the LAB at approximately 14 s (Li *et al.* 2000) which is also identified in Fig. 5 (labelled LVZ). This phase, proposedly, originates at the top of a LVZ at 130–140 km depth. Previously, this has been interpreted as a zone of water-rich and low-degree partially melted peridotite within the central hot part of the plume (Li *et al.* 2000). Recently, a more extensive model for melt generation has been developed. Accordingly, eclogite bodies, that is, recycled oceanic crust, are rising within the plume conduit. Due to its lower solidus the eclogite would melt in the proposed depth range infiltrating into and reacting with the ambient peridotite, so solid pyroxenite is produced (Sobolev *et al.* 2005).

We investigate more precisely the extent of the LVZ. Data with high signal-to-noise ratio recorded on the Big Island are selected and manually sorted into two subsets. The first contains 130 traces

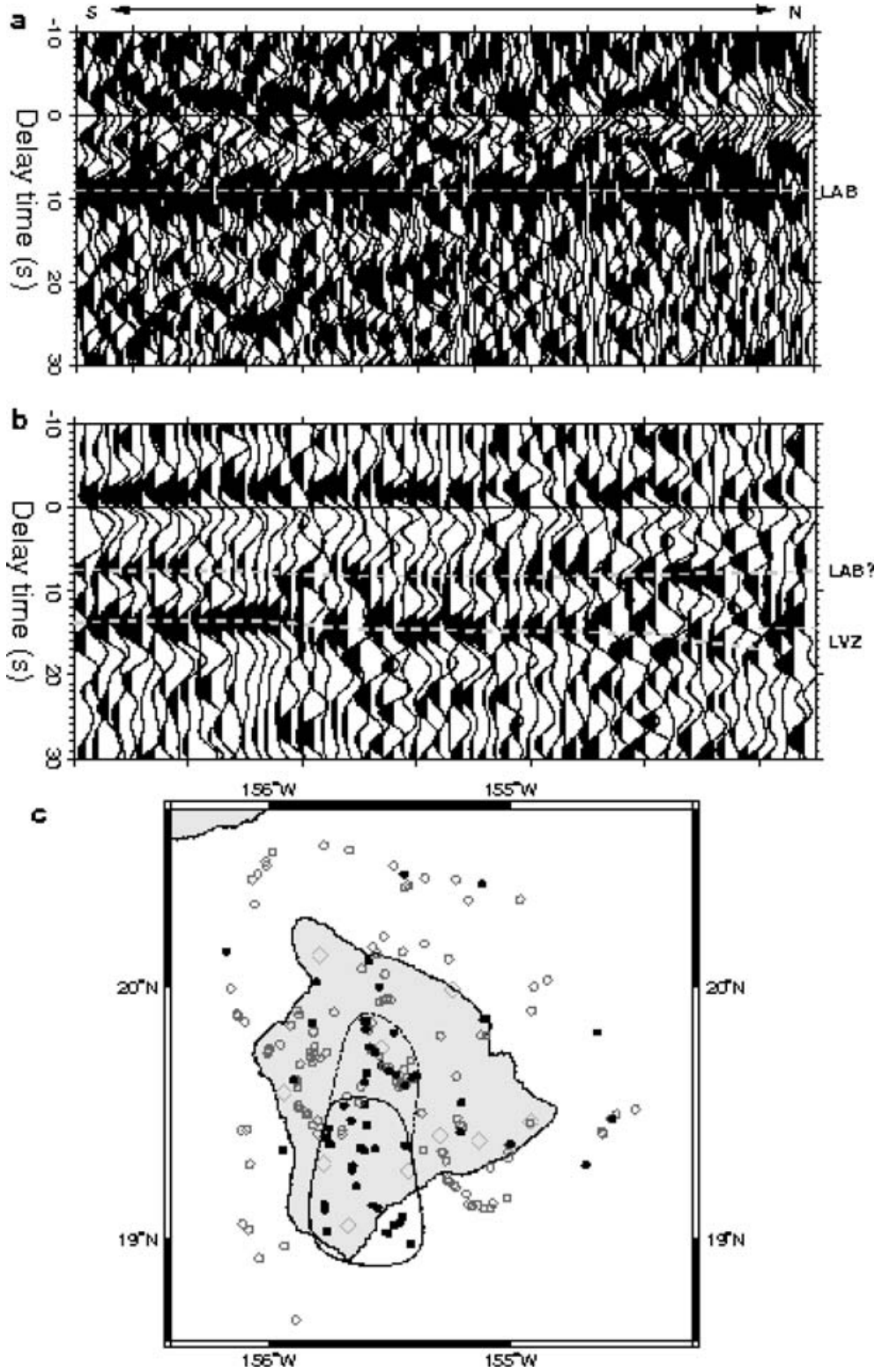

Figure 7. Equally spaced receiver functions recorded at stations on Big Island. Traces are bandpass filtered from 5 to 30 s and sorted by latitude of related piercing points in 100 km depth. We manually divide the data set regarding the occurrence of a negative phase at about 14 s. Section (a) shows traces with a negative phase at about 9 s interpreted as conversions from the LAB, but no coherent signal can be found at 14 s. (b) The bottom section is dominated by strong converted phases at about 14 s, whereas the presumable LAB phase now occurs at about 7 s. In (c) the related piercing points at a depth of 140 km are shown. Open circles correspond to traces showing LAB converted phases only, and solid circles locate piercing points of traces exhibiting an additional phase at about 14 s. The latter concentrate most within the area bordered by the solid line, but the area may also extend further to the north (dashed line). Station locations are indicated with open diamonds.

showing only the LAB phase, whereas the second one consists of 64 traces exhibiting the additional signal. Sections of single receiver functions are compared in Figs 7(a) and (b). We apply a bandpass filter from 5 to 30 s. Traces are equally spaced and sorted by latitude of the corresponding piercing points calculated for a depth of 140 km. In Fig. 7(a) strong LAB converted phases can be detected at delay times slightly varying around 9 s (denoted by the dashed line). In Fig. 7(b), an additional negative phase occurs at about 14 s (LVZ). This phase is less distinctive than the LAB in Fig. 7(a), and the LAB phase is weaker as discussed in the previous section. The distribution of piercing points of both subsets is presented in Fig. 7(c). Even though we select only a relatively small number of receiver functions from the original data, good coverage is obtained. Piercing points of traces containing LAB signal only are denoted with open circles, whereas solid circles designate the occurrence of the 14 s phase. Solid circles notably accumulate in the central to the southwestern part of Big Island. The solid line in Fig. 7(c) outlines the area where solid circles are most concentrated. Approximately 89 per cent of the computed receiver functions within this zone possess the additional phase. We assume this area of about 75 × 50 km to be the central part of the observed LVZ at 140 km. We estimate the lateral resolution of a single receiver function from the first Fresnel zone, which in this case is roughly 50 km. Many solid circles are located further to the north, so the proposed area may possibly expand to 120 × 50 km as suggested by the dashed line. Here, the fraction of traces indicating the LVZ is about 70 per cent, and approximately 76 per cent of all piercing points related to the receiver functions shown in Fig. 7(b) are situated within this extended area. Admittedly, a number of solid circles are spread all over the surrounding region. Potentially, we select some of the corresponding receiver functions displayed in Fig. 7(b) by mistake as they do not show a clear LAB phase, but also no significant phase at 14 s. We have to consider, also, that converted energy from a fairly large Fresnel zone contributes to the seismic signal rather than being generated at a single point (Sheriff 1980).

3.4 Mantle transition zone

The MTZ is defined by the major seismic discontinuities at *ca.* 410 and 660 km depth according to IASP91 reference earth model (Kennett & Engdahl 1991). The mantle discontinuities are related to mineral phase changes mainly in the olivine system (e.g. Bina & Helffrich 1994; Helffrich & Wood 2001). They are of special interest for mantle plumes due to their diametrical pressure-temperature relation. Compared to IASP91 thinning of the MTZ by about 14 km is observed in a corridor Tonga-Hawaii in the central Pacific (Gaherty *et al.* 1996). Li *et al.* (2000) discovered an updoming of the 660 km discontinuity by 40 to 50 km SW of Big Island using receiver functions. This is confirmed by another receiver function study furthermore suggesting extended thinning of the MTZ in an area about 700 km along the southern flank of the Hawaii swell (Collins *et al.* 2002). However, both observations are only documented by sparse data sets.

We investigate in greater detail the topography of the major mantle discontinuities underneath the southernmost part of the Hawaiian chain. Moveout correction is applied to the data as described in Section 2. We stack the traces in boxes of 0.7° × 0.7° (not shown) according to the position of the related piercing points, separately, at 410 and 660 km depth. Delay times of mantle phases (P_{410}s and P_{660}s) are derived for each stacking box, however, results are not able to reliably image small-scale topography of the mantle discontinuities. The number of traces summed in each box has proven too small to sufficiently suppress noise. Furthermore, the box width is in the order of the first Fresnel zone, which is limiting the resolution. Using a bandpass from 2 to 30 s for a single trace its dimension is about 65 and 86 km at 410 and 660 km depth, respectively. A bandpass from 10 to 30 s increases the dimension of the Fresnel zone to approximately 146 and 194 km, respectively. This is roughly twice the binning width. However, we deduce fundamental tendencies from the summed traces. Thus, for further investigation we define three zones (SE, Plume, NW) shown in Fig. 8(a).

We select about 40 per cent of all single traces for high signal-to-noise ratio. Fig. 8(a) presents the distribution of the corresponding piercing points at a depth of 660 km. We stack all receiver functions within the three zones mentioned above and apply a bandpass filter from 2 to 30 s. Resulting sum traces are shown in Fig. 8(b) and arrivals generated at the major discontinuities are indicated (grey ticks). We select 10 subsets of traces in each zone and use the bootstrap method (Efron & Tibshirani 1986) as described in Section 2 to verify coherent phases (Fig. 9). Theoretical delay times according to IASP91 for the discontinuities at 410 and 660 km depth (hereafter referred to as the 410 and the 660, respectively), that is, 44.1 and 68.1 s respectively, are denoted by thin black lines in both figures. We derive average delay times of the observed mantle phases from the sum traces in Fig. 8(b), which are based on the rightmost traces in Figs 9(a)–(c). We use the variations of delay times to roughly estimate a medium value and standard deviation of arrivals for the discontinuities in each zone. The area SE of Big Island is sparsely sampled with only 76 traces contributing to the stack. Averaged mantle phases, however, can be detected (Fig. 8b, right, and Fig. 9c). We obtain delay times of about 44.5 ± 0.5 s and 67.7 ± 0.4 s for P_{410}s and P_{660}s, respectively, indicating only minor deviation from IASP91 values. The encircled zone SW of Big Island in Fig. 8(a) is the area of the plume reported previously (Li *et al.* 2000). Here, the mantle phases (Fig. 8b, middle, and Fig. 9b) occur at 46.7 ± 0.3 s and 68.3 ± 0.4 s, respectively, that is, the differential time is decreased by approximately 2.5 s. The NW zone, finally, exhibits a delay of both mantle phases. From the bottom trace in Figs 8(b) and 9(a) we derive 47.0 ± 0.4 s and 71.0 ± 0.2 s, respectively.

The estimate of the standard deviation depends on the filter applied. We test the effects of different filters on delay times obtained for mantle phases. Results are presented in Fig. 10 in terms of differential delay times versus P_{410}s phases and compared with results from a previous study of transition zone thicknesses (Li *et al.* 2003b). Circles mark the mean values for the three zones with bars indicating the range obtained from different bandpass filters.

(1) In the SE zone delay times of the mantle phases almost agree with theoretical times derived from IASP91. Obviously, the plume has not yet influenced the MTZ underneath the youngest part of the Hawaiian swell.

(2) SW of Big Island is suggested to be the plume zone. Here, differential times of mantle phases are decreased by about 2 s compared to IASP91 as expected in the presence of hot upwelling material.

(3) The NW part of the study area, that is, between Big Island and Kauai, reveals mantle phases delayed by about 3 s without significant decrease of differential time. As arrivals of both discontinuities are equally affected this delay must originate above the MTZ, which can be explained by a channel of reduced *S*-wave velocity along the island chain. This would be a likely consequence of the hot plume material dragged off by the moving plate mentioned in Section 3.2.

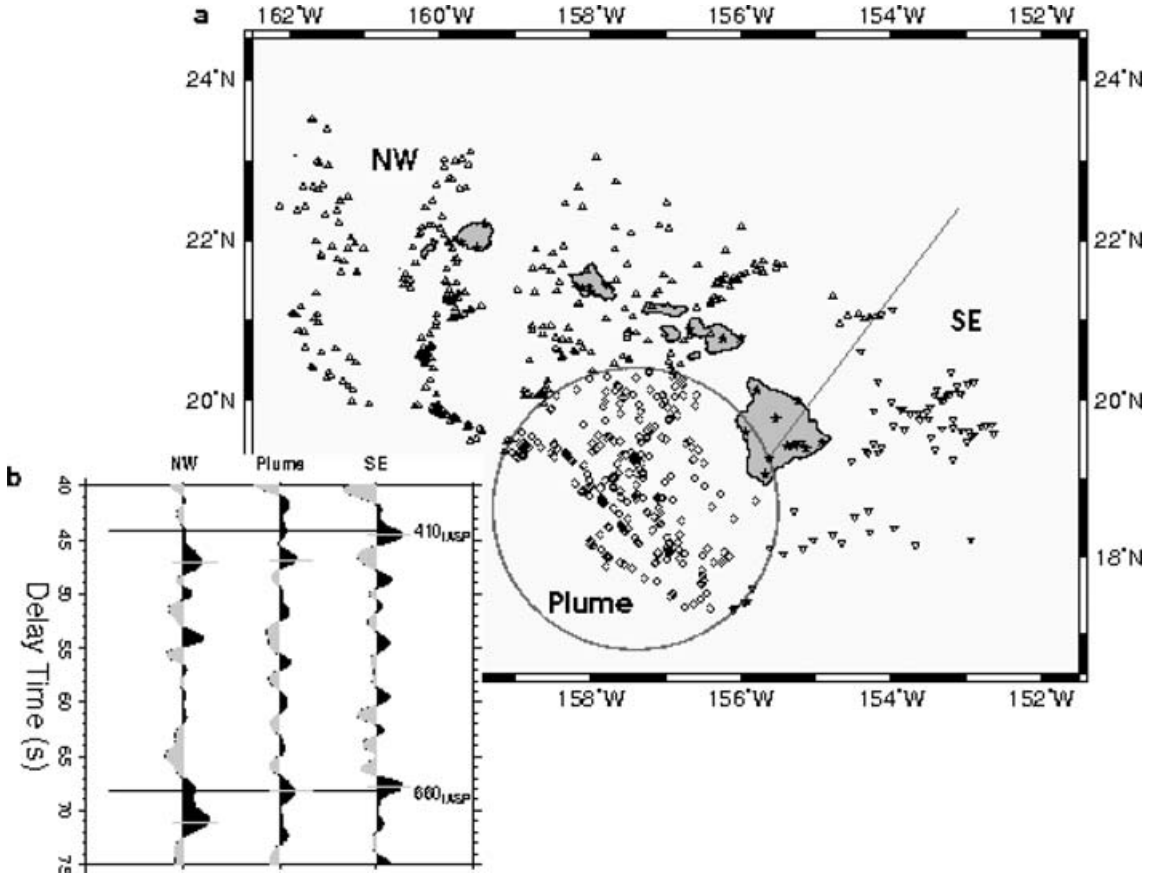

Figure 8. (a) Distribution of piercing points computed at a depth of 660 km. We use only the 690 traces possessing the best signal-to-noise ratios. The study area is divided into three regions: The encircled area marks the inferred position of the plume conduit at 660 km (diamonds). A radius of 200 km is adopted from a previous study (Li *et al.* 2000). Southeast of the straight line (inverse triangles) arrival times of P_{410}s and P_{660}s phases relative to *P* onset are in good agreement with the IASP91 model, whereas the region northwest (triangles) reveals significant delay of both upper mantle phases P_{410}s and P_{660}s (see also Figs 9 to 11). (b) Sum traces corresponding to the three zones described in (a). Traces are bandpass filtered from 2 to 30 s, and a moveout correction for a reference slowness of 6.4 s/° is applied before summation. The traces (from left to right) represent the mantle phases obtained in the SE part of the study area, in the plume zone and in the NW part of the investigated area, respectively. Theoretical delay times of major mantel phases relative to *P* onset are marked with respect to IASP91.

The radius of the plume conduit has previously been estimated to be about 200 km (Li *et al.* 2000). In Fig. 11 we show sum traces for varying plume radius with a fixed centre. Here, we sum traces according to the piercing points at 660 km depth. The P_{660}s phase shows minimum arrival time of about 67.1 s after *P* onset at radii up to 120 km. We interpret this to be the hot core of the plume conduit. The delay time increases with radius because of declining temperature of the inferred conduit. The radius indicates a deep lower mantle plume source rather than a thermal boundary layer directly underneath the transition zone, which would affect a much broader region of the 660 (Shen *et al.* 1998). The P_{660}s phase is followed by additional signals possibly originating either outside the plume conduit or at an additional interface (see also Fig. 12). The P_{410}s phase gives a constant delay time irrespective of the chosen plume radius. This is likely explained by the distribution of the underlying piercing points, which is NE to those of the 660. Most of the sum traces in Fig. 11 show a second signal arriving about 4.3 s after the main P_{410}s phase. The P_{520}s phase would be expected approximately 10 s after P_{410}s and, therefore, can be ruled out as the reason for this phase. Excess temperature in the vicinity of the plume would even increase its delay time due to the high positive Clapeyron slope of the 520 km discontinuity (Katsura *et al.* 2004). We suggest, that the second arrival is the P_{410}s phase generated inside the plume conduit. The former, in contrast, originates outside the conduit, thus, only exhibiting the same delay time as in the NW zone.

We verify lateral delay time variations of the mantle phases by summing traces along the island profile. For the binning procedure we select overlapping circular areas of 150 km radius moving along the profile in steps of 50 km (sliding window technique). To account for different piercing point distribution, we apply separate binning for both discontinuities. In Fig. 12(a) distributions of piercing points computed for 410 km depth (top) and 660 km depth (bottom) are displayed. Piercing points calculated for a depth of 410 km are located closer to the swell axis, thus, we choose a profile with 15 positions along the island chain for binning at this depth. Based on the plume position in Fig. 8, we sum along a profile SW of the Hawaiian islands at depth of 660 km. We show 20 s sum traces of the 410 and 660 profiles in Fig. 12(b). Theoretical delay times of mantle phases according to IASP91 model are denoted by thin lines. The P_{410}s and P_{660}s phases are marked with thick solid lines. The section confirms the results in Fig. 8(b) reproducing the three major zones with the NW showing mantle phases both delayed by about 3 s. Mantle phases deflected by the plume conduit are emphasized by dashed lines. Earliest P_{660}s arrivals are found SW of Big Island in agreement with the findings mentioned above. However, there is no

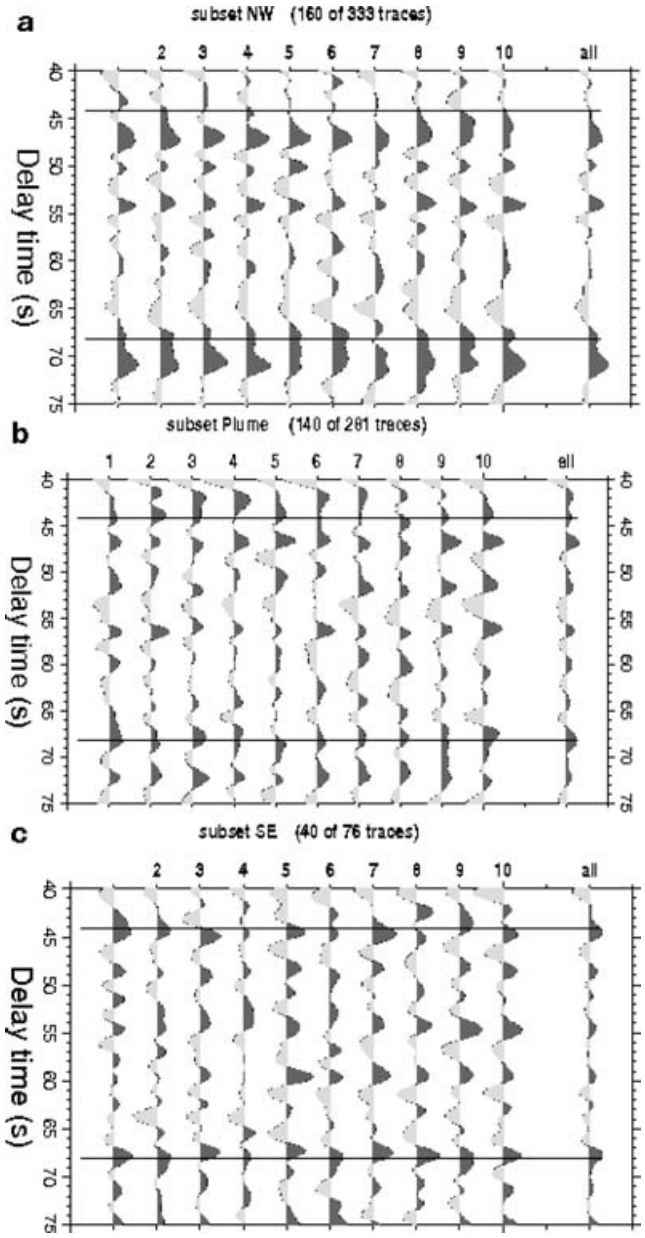

Figure 9. Bootstrap sections for the areas defined in Fig. 8. (a–c) represent the three regions in the same order as in Fig. 8(b): the southeast (a), the plume zone (b) and the northwest (c), respectively. For every region we select and stack 10 subsets of about half the total number. In each section, to the right, the same sum trace of the region is presented as in Fig. 8(b) but using a different scale.

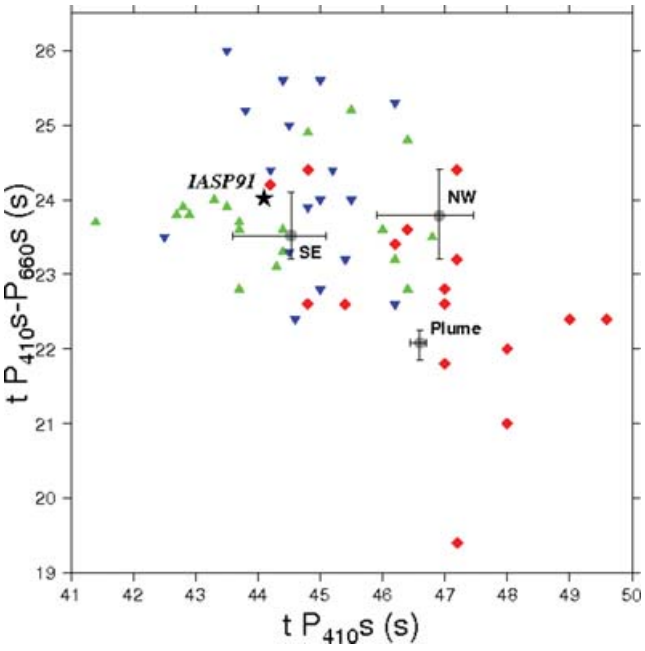

Figure 10. Diagram of differential traveltimes of the mantle phases versus P_{410}s arrivals. Circles denote the average values obtained for the three areas derived from 8 different bandpass filters ranging from 0.33–30 s to 12–30 s. The bars mark the range of variations. The grey circles designate the NW, the plume zone and the SE, respectively. Obvious outliers have been removed before averaging. The theoretical value according to IASP91 model is marked by the asterisk. For comparison, results from Li *et al.* (2003a) have been plotted in colour. Red diamonds show other plume areas mainly from the Pacific, whereas blue inverse triangles mark locations in the oceanic NW Pacific. Green triangles are for continental sites in North America.

evidence for an extended zone of significant thinning of the MTZ along the Hawaiian swell as proposed by Collins *et al.* (2002). The binning at depth of 410 km, shows a downwelling zone of the interface in parallel to the 660. In a couple of bins both, the generally delayed, as well as the downwardly deflected P_{410}s phase occur, due to the plume position SW to Big Island. Thus, the bins at 410 km depth also samples regions outside the plume conduit. In the SE, P_{410}s phase approaches the theoretical time (IASP91).

Additional coherent phases are detected in the binning section (dotted lines in Fig. 12b). First of which occurs at approximately 43 s after *P* onset, slightly increasing to the SE. The signal is strong in the NW fading away in the area of Oahu. We stack the traces once again after applying a moveout correction for multiple phases (not shown). This enhances the multiple signal. Considering a general delay of approximately 3 s the observed time would correspond either to a PpPs multiple generated at 115 km or to *PpSs*/*PsPs* multiples with reversed polarity originating at a depth of about 85 km. While we observe no direct conversion related to the former depth, the latter is in acceptable agreement with the depth to LAB outside or in the periphery of the heated channel mentioned above, also showing correct polarity. Therefore, we associate this signal to *PpSs* and *PsPs* multiple phases generated at the LAB.

A second additional phase occurs at about 67 s at the NW increasing to about 69 s further SE and merging with the P_{660}s phase in the assumed plume zone. Again, a multiple phase is indicated. Theoretical receiver functions (Li & Yuan 2003) demonstrate the occurrence of a PpPs multiple phase generated at the Lehmann discontinuity within the time range of the P_{660}s arrival. Incorporating the general delay the observed arrival times roughly correspond to a depth of 185 to 190 km. This lies within the depth range to the Lehmann discontinuity derived from precursors to PP in the northwest Pacific (Rost & Weber 2001). We suggest, that the observed multiple phase originates at the Lehmann discontinuity. Although, we cannot detect the related direct converted phase which is covered by strong shallow multiples. Approaching the plume zone the assumed Lehmann multiple interferes with the P_{660}s phase. A weak signal continues towards SE which, supposedly, consists of two superposed phases similar to the sum trace corresponding to 150 km radius in Fig. 11. At smaller radii, in Fig. 11, two phases can be resolved following the P_{660}s, however, it is difficult to verify their

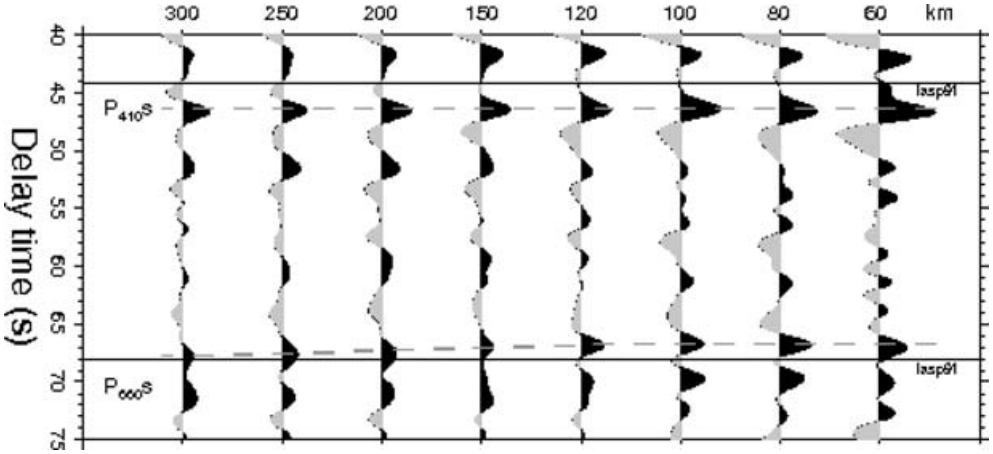

Figure 11. Comparison of sum traces acquired at varying conduit radii. Traces are summed according to piercing points at 660 km depth in which the plume centre is kept fixed as shown in Fig 8(a). Theoretical delay times for mantle phases according to IASP91 are marked with thin lines. Dashed lines indicate observed mantle phases. The P_{410}s phase is detected consistently at about 47 s, whereas the P_{660}s phase occurs at delay times of about 67 s for radii up to 120 km increasing as the radius is increased. Radii are given in km (top).

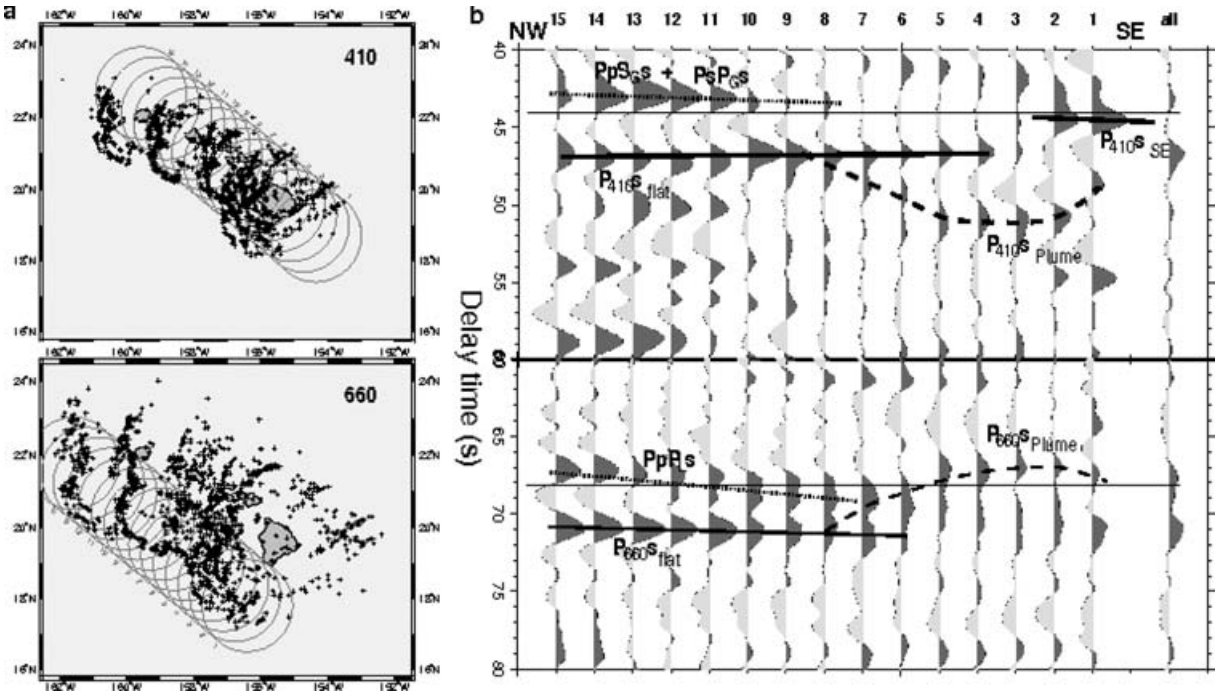

Figure 12. (a) Distribution of piercing points (marked by crosses) computed for upper mantle discontinuities at depth of 410 km (top) and 660 km (bottom). Overlapping circles denote binning areas selected for sliding window technique shown in (b). Circles have a radius of 150 km. Numbers are corresponding to the numbered sum traces in (b). The profile at 660 km (bottom) has been shifted to the southern flank of the Hawaii swell according to the updoming area southwest of Big Island. (b) Sliding window section related to locations shown in (a). Traces are filtered with a bandpass 2 to 30 s and separately binned for 410 km (40 to 60 s) and 660 km (60–80 s) discontinuities to account for different piercing point distribution. Thin lines indicate theoretical arrivals according to IASP91. Direct mantle phases P_{410}s and P_{660}s (marked by solid lines) are generally delayed by about 3 s in the NW parts of both profiles. P_{410}s approaches the IASP91 arrival time in the SE. Dashed lines indicate deflected mantle discontinuities caused by the impinging plume. In addition (denoted by dotted lines), a phase at approximately 43 s (labelled $PpS_{GS}s + PsP_{GS}s$) is interpreted as a secondary multiple phase from the LAB or Gutenberg discontinuity, whereas the phase at 67 to 68 s (labelled PpP_Ls) could be explained as a multiple phase from the Lehmann discontinuity at about 185 to 190 km depth.

origin. One of which might be related to the Lehmann multiple. The second phase could be explained by the mineral phase transition in the garnet system possibly causing a seismic discontinuity (also referred to as 710 km discontinuity), which has a Clapeyron slope of opposite sign compared to the breakdown of ringwoodite (e.g. Vacher *et al.* 1998; Simmons & Gurrola 2000). In the plume conduit the majorite–perovskite transition would deepen, while the 660 km discontinuity is upwelling. However, we have to consider, that P_{660}s arrivals originating outside the plume conduit may also contribute to the signal at later arrival times.

We estimate the excess temperature of the plume from arrival time changes. We assume the observed mean arrival time of 47.0 s to correspond to normal depth of the 410. In the plume zone we obtain a delay time of about 4.3 s which is approximately equivalent

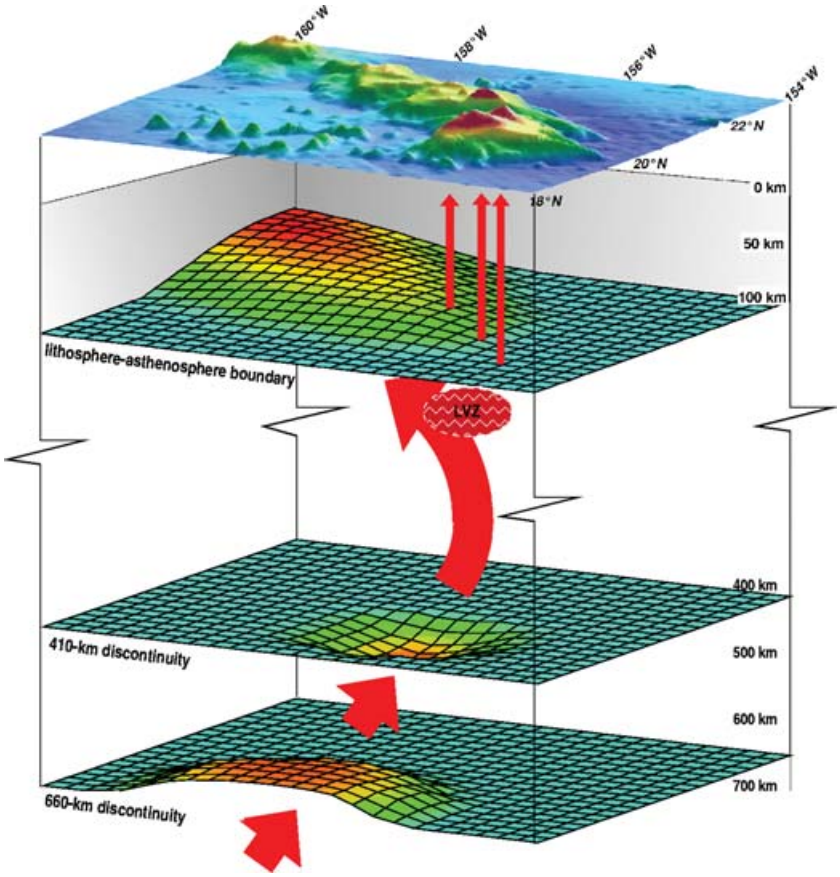

Figure 13. Schematic model of the upper mantle underneath Hawaii summarizing the observed effects of the plume on seismic discontinuities. Temperature increase at the interfaces is indicated by yellow to red colours. Red arrows suggest the position of the tilted plume conduit which penetrates the mantle transition zone southwest of Big Island. Plume material hits the lithosphere and is dragged off by the moving plate, while only a small amount rises through the lithosphere.

to 45 km increase in depth. In previous studies a Clapeyron slope of about 2.9 MPa K^{-1} has been suggested (e.g. Bina & Helffrich 1994), which would result in an excess temperature of approximately 500 K. Katsura *et al.* (2004) propose a Clapeyron slope of 4 MPa K^{-1} roughly leading to 375 K. This seems more likely in terms of plume dynamics as discussed by Korenaga (2005). In the NW the mean P_{660}s arrival time is 71.0 s occurring about 3.9 s earlier inside the plume zone, which corresponds to shallowing of the 660 of approximately 60 km. Given a Clapeyron slope of -2 MPa K^{-1} (Bina & Helffrich 1994) would result in an excess temperature of about 1350 K which is obviously unrealistic. However, the mean arrival time is based on the general delay of 3 s relative to IASP91 caused by the channel of dragged plume material. The delay time should decrease or even vanish to the SE in view of the ray paths missing that channel or passing through a thinner part. Since the exact portion and distribution of dragged material is unknown, we are not able to deduce the exact depth change of the 660.

Fig. 13 schematically summarizes our results: The plume rises from the lower mantle and penetrates the transition zone SW of Big Island and further ascends in a narrow conduit tilted towards the NE. At depth range between about 170 and 140 km a zone of partial melting develops within the conduit seismically observable as a LVZ. When impinging the lithosphere a large amount of hot plume material is dragged off by the overriding plate forming a hot trail, characterized by reduced *S*-wave velocities and also causing lithospheric thinning. A small amount of the plume material penetrates the lithosphere thus causing hotspot volcanism.

4 CONCLUSIONS

The crust and the upper mantle beneath Hawaii are investigated in greater detail than before using receiver functions. The study reveals a strong shallow intracrustal structure in the SE weakening towards NW while increasing in depth. The structure very likely relates to volcanic causes. We also find strong signal on the transverse components. At station KIP on Oahu a 360° periodicity is revealed which can be explained either as an interface dipping by 20°, as a 10 per cent anisotropic layer with a dipping symmetry axis in the lower crust or by local 3-D heterogeneities caused by volcanic structures. We confirm lithospheric thinning increasing towards NW along the island chain. Our results indicate, that thinning extends at least to the island of Midway, about 2000 km NW of Hawaii, where the LAB is found at depth similar to Kauai. Generally delayed arrivals of the mantle phases P_{410}s and P_{660}s in the NW support the idea of a channel of hot plume material along the island chain dragged off by the overriding plate.

The dimensions of an asthenospheric LVZ are determined, which is located in the SW part of Big Island. Further to the SW, we verify upwelling of the 660 and, for the first time, downwelling of the

410 with the latter demonstrating elevated temperatures by approximately 375 K at depth of the MTZ. From the position SW of Big Island we infer, that the plume conduit is tilted towards the NE. The plume is located off axis of the island chain at depth of the MTZ indicating either a shift in direction of plate motion as proposed, for example, by Wessel & Kroenke (1997) and Cox (1999) or motion of the plume conduit itself as previously suggested (e.g. Tarduno *et al.* 2003; Parés & Moore 2005). Passing through a viscous mantle the plume conduit is supposed to be bended and tilted into the direction of mantle flow which is identical to the direction of plate motion in the upper mantle (Cox 1999). The Hawaiian plume, instead, is located behind the recent volcanism at depth of the MTZ. Thus, the tilt direction of the conduit is contrary to the plate motion. Steinberger *et al.* (2004) have modelled a large-scale mantel flow field suggesting southward motion of the Hawaii plume which, indeed, predicts the off axis position of the conduit. However, the model is not in agreement with the observed longitude of the plume at the 660. To explain the eastward shift of the rising plume we assume decoupling of lower and upper mantle convection in the area of Hawaii including backward flow at the base of the upper mantle.

ACKNOWLEDGMENTS

This research project was supported by the Deutsche Forschungsgemeinschaft (DFG) within the framework of the International Continental Drilling Project (ICDP). We would like to thank IRIS, GEOSCOPE and USGS for making additional data available to us. Data have been processed using the SeismicHandler software package (Stammler 1993). The majority of figures have been made using Generic Mapping Tools (Wessel & Smith 1998). The manuscript benefited much from the comments of two anonymous reviewers.

REFERENCES

Bina, C.R. & Helffrich, G.R., 1994. Phase transition Clapeyron slopes and transition zone seismic discontinuity topography, *J. geophys. Res.,* **99,** 15 853–15 860.

Bock, G., 1991. Long-Period S to P Converted Waves and the Onset of Partial Melting Beneath Oahu, Hawaii, *Geophys. Res. Lett.,* **18,** 869–872.

Budweg, M., Bock, G. & Weber, M., 2006. The Eifel Plume—imaged with converted waves, *Geophys. J. Int.,* doi:10.1111/j.1365-246X.2005.02778.x.

Collins, J.A., Vernon, F.L., Orcutt, J.A. & Stephen, R.A., 2002. Upper mantle structure beneath the Hawaiian swell: constraints from the ocean seismic network pilot experiment, *Geophys. Res. Lett.,* **29,** doi:10.1029/2001GL013302.

Cox, R.T., 1999. Hawaiian volcanic propagation and Hawaiian swell asymmetry: evidence of northwestward flow of the deep upper mantle, *Tectonophysics,* **310,** 69–79.

Crosson, R.S. & Koyanagi, R.Y., 1979. Seismic velocity structure below the Island of Hawaii from local earthquake data, *J. geophys. Res.,* **84,** 2331–2342.

Cserepes, L. & Yuen, D.A., 2000. On the possibility of a second kind of mantle plumes, *Earth planet. Sci. Lett.,* **183,** 61–71.

Cserepes, L., Yuen, D.A. & Schroeder, B.A., 2000. Effect of the mid-mantle viscosity and phase-transition structure on 3D mantle convection, *Phys. Earth planet. Inter.,* **118,** 135–148.

Davaille, A., Girard, F. & Le Bars, M., 2002. How to anchor hotspots in a convecting mantle?, *Earth planet. Sci. Lett.,* **203,** 621–634.

Detrick, R.S. & Crough, S.T., 1978. Island Subsidence, Hot Spots, And Lithospheric Thinning, *J. geophys. Res.,* **83,** 1236–1244.

Efron, B. & Tibshirani, R., 1986. Bootstrap methods for standard errors, confidence intervals and other measures of statistical accuracy, *Stat. Sci.,* **1,** 54–77.

Fee, D. & Dueker, K., 2004. Lowermost mantle anisotropy beneath the Pacific: Imaging the source of the Hawaiian plume, *Geophys. Res. Lett.,* **190,** 167–180.

Fouch, M.J., Fischer, K.M. & Wysession, M.E., 2001. Lowermost mantle anisotropy beneath the Pacific: imaging the source of the Hawaiian plume, *Earth planet. Sci. Lett.,* **190,** 167–180.

Gaherty, J.B., Jordan, T.H. & Gee, L.S., 1996. Seismic structure of the upper mantle in a central Pacific corridor, *J. geophys. Res.,* **101,** 22 291–22 309.

Helffrich, G.R. & Wood, B.J., 2001. The earth's mantle, *Nature,* **412,** 501–507.

James, D.E. & Savage, M.K., 1990. A search for seismic reflections from the top of the oceanic crust beneath Hawaii, *Bull. seism. Soc. Am.,* **80,** 675–701.

Jones, C.H. & Phinney, R.A., 1998. Seismic structure of the lithosphere from teleseismic converted arrivals observed at small arrays in the southern Sierre Nevada and vicinity, California, *J. geophys. Res.,* **103,** 10 065–10 090.

Katsura, T. *et al.,* 2004. Olivin-wadsleyite transition in the system (Mg, Fe)$_2$SiO$_4$, *J. geophys. Res.,* **109,** B02209, doi:10.1029/2003JB002438.

Kennett, B. & Engdahl, E., 1991. Travel times for global earthquake location and phase identification. *Geophys. J. Int.,* **105,** 429–465.

Korenaga, J., 2005. Firm mantle plumes and the nature of the core-mantle boundary region. *Earth planet. Sci. Lett.,* **232,** 29–37.

Laske, G., Morgan, J.P. & Orcutt, J.A., 1999. First results from the Hawaiian SWELL Pilot Experiment, *Geophys. Res. Lett.,* **26,** 3397–3400.

Levin, V. & Park, J., 1997. P–SH conversions in a flat-layered medium with anisotropy of arbitrary orientation, *Geophys. J. Int.,* **131,** 253–266.

Li, X. & Yuan, X., 2003. Receiver Functions in northeast China—implications for slab penetration into the lower mantle in northwest Pacific subduction zone, *Earth planet. Sci. Lett.,* **216,** 679–691.

Li, X., Kind, R., Priestley, K., Sobolev, FS.V., Tilman, F., Yuan, X. & Weber, M., 2000. Mapping the Hawaiian plume conduit with converted seismic waves, *Nature,* **405,** 938–941.

Li, X., Kind, R. & Yuan, X., 2003a. Seismic study of upper mantle transition zone beneath hotspots, *Phys. earth Planet. Inter.,* **136,** 79–92.

Li, X., Kind, R., Yuan, X., Sobolev, S.V., Hanka, W., Ramesh, D.S., Gu, Y. & Dziewonski, A.M., 2003b. Seismic observation of narrow plumes in the oceanic upper mantle, *Geophys. Res. Lett.,* **30,** 1334, doi:10.1029/2002GL015411.

Li, X., Kind, R., Yuan, X., Wölbern, I. & Hanka, W., 2004. Rejuvenation of the lithosphere by the Hawaiian plume, *Nature,* **427,** 827–829.

Lindwall, D.A., 1988. A Two-Dimensional Seismic Investigation of Crustal Structure Under the Hawaiian Islands Near Oahu and Kauai, *J. geophys. Res.,* **93,** 12 107–12 122.

Marquart, G. & Schmeling, H., 2000. Interaction of small mantle plumes with spinel-perovskite phase boundary: implications for chemical mixing, *Earth planet. Sci. Lett.,* **177,** 241–254.

McCowan, D.W. & La Coss, R.T., 1978. Transfer function for three seismic research observatory system, *Bull. seism. Soc. Am.,* **68,** 501–512.

McNamara, A.K. & Zhong, S., 2004. The influence of thermochemical convection on the fixity of mantle plumes, *Earth planet Sci. Lett.,* **222,** 485–500.

Montelli, R., Nolet, G., Dahlen, F.A., Masters, G., Engdahl, E.R. & Hung, S.-H., 2004. Finite-frequency tomography reveals a variety of plumes in the mantle, *Science,* **303,** 338–343.

Morgan, W.J., 1971. Convection plumes in the lower mantle, *Nature,* **230,** 42–43.

Norton, I.O., 1995. Plate motions in the North Pacific: The 43 Ma nonevent, *Tectonics,* **14,** 1080–1094.

Parés, J.M. & Moore, T.C., 2005. New evidence for the Hawaiian hotspot plume motion since the Eocene, *Earth planet. Sci. Lett.,* **237,** 951–959.

Pietruszka, A.J. & Garcia, M.O., 1999. The size and shape of Kilauea's Volcano's summit magma storage reservoir: a geochemical probe, *Earth planet. Sci. Lett.,* **167,** 311–320.

Priestley, K. & Tilmann, F., 1999. Shear-wave structure of the lithosphere above the Hawaiian hot spot from two-station Raleigh wave phase velocity measurements, *Geophys. Res. Lett.,* **26,** 1493–1496.

Ribe, N.M., 2004. Through thick and thin, *Nature,* **427,** 793–795.

Ritsema, J. & Allen, R.M., 2003. The elusive mantle plume, *Earth planet. Sci. Lett.,* **207,** 1–12.

Rost, S. & Weber, M., 2001. A reflector at 200 km depth beneath the northwest Pacific, *Geophys. J. Int.,* **147,** 12–28.

Russel, S.A., Lay, T. & Garnero, E.J., 1998. Seismic evidence for small-scale dynamics in the lowermost mantle at the root of the Hawaiian hotspot, *Nature,* **396,** 255–258.

Savage, M.K., 1998. Lower crustal anisotropy or dipping boundaries? Effects on receiver functions and a case study in New Zealand, *J. geophys. Res.,* **103,** 15 069–15 087.

Seidler, E., Jacoby, W. & Cavsak, H., 1999. Hotspot distribution, gravity, mantle tomography: evidence for plumes, *J. Geodyn.,* **27,** 585–608.

Shen, Y., Solomon, S.C., Bjarnason, I.T. & Wolfe, C.J., 1998. Seismic evidence for a lower-mantle origin of the Iceland plume, *Nature,* **395,** 62–65.

Sheriff, R.E., 1980. Nomogram for Fresnel-zone calculation, *Geophysics,* **45,** 968–972.

Simmons, N.A. & Gurrola, H., 2000. Multiple seismic discontinuities near the base of the transition zone in the Earth's mantle, *Nature,* **405,** 559–562.

Sobolev, A.V., Hoffmann, A.W., Sobolev, S.V. & Nikogosian, I.K., 2005. An olivine-free mantle source of Hawaiian shield basalts, *Nature,* **434,** 590–597.

Sobolev, S.V., Zeyen, H., Granet, M., Achauer, U., Bauer, C., Werling, F., Altherr, R. & Fuchs, K., 1997. Upper mantle temperatures and lithosphere-asthenosphere system beneath the French Massif Central constrained by seismic, gravity, petrologic and thermal observations, *Tectonophysics,* **275,** 143–164.

Stammler, K., 1993. SeismicHandler—programmable multichannel data handler for interactive and automatic processing of seismological analysis, *Comp. Geosci.,* **19,** 135–140.

Steinberger, B., 2000. Plumes in a convecting mantle: Models and observations for individual hotspots, *J. geophys. Res.,* **105,** 11 127–11 152.

Steinberger, B., Sutherland, R. & O'Connell, R.J., 2004. Prediction of Emperor-Hawaii seamount locations from a revised model of global plate motion and mantle flow, *Nature,* **430,** 167–173.

Stock, J., 2003. Hotspots Come Unstuck, *Science,* **301,** 1059–1060.

Tarduno, J.A. & Cotrell, R.D., 1997. Paleomagnetic evidence for motion of the Hawaiian hotspot during formation of the Emperor seamounts, *Earth planet. Sci. Lett.,* **153,** 171–180.

Tarduno, J.A. *et al.,* 2003. The Emperor seamounts: southward motion of the Hawaiian hotspot plume in Earth's mantle, *Science,* **301,** 1064–1069.

Vacher, P., Mocquet, A. & Sotin, C., 1998. Computation of seismic profiles from mineral physics: The importance of non-olivine components for explaining the 660 km depth discontinuity, *Phys. Earth planet. Inter.,* **106,** 275–298.

Wang, S. & Wang, R., 2001. Current plate velocities relative to hotspots: implications for hotspot motion, mantle viscosity and global reference frame, *Earth planet. Sci. Lett.,* **189,** 133–140.

Wang, Z., Kitchen, N.E. & Eiler, J.M., 2003. Oxygen isotope geochemistry of the second HSDP core, *Geochem. Geophys. Geosyst.,* **4**(8), 8712, doi:10.1029/2002GC000406.

Wessel, P. & Kroenke, L., 1997. A geometric technique for relocating hotspots and refining absolute plate motions, *Nature,* **387,** 365–369.

Wessel, P. & Smith, W.H.F., 1998. New, improved version of the Generic Mapping Tool released, *EOS. Trans. Am. geophys. Un.,* **79,** 579.

Wilson, J.T., 1963. Evidence from islands on the spreading of the ocean floor, *Nature,* **197,** 536–538.

Woods, M.T. & Okal, E.A., 1996. Rayleigh-wave dispersion along the Hawaiian Swell: A test of lithospheric thinning by the thermal rejuvenation at a hotspot, *Geophys. J. Int.,* **125,** 325–339.

Woods, M.T., Leveque, J.J. & Okal, E.A., 1991. Two-station measurements of Rayleigh wave group velocity along the Hawaiian swell, *Geophys. Res. Lett.,* **18,** 105–108.

Yuan, X., Ni, J., Kind, R., Mechie, J. & Sandvol, E., 1997. Lithospheric und upper mantle structure of southern Tibet from a seismological passive source experiment, *J. geophys. Res.,* **102,** 27 491–27 500.

Zhao, D., 2001. Seismic structure and origin of hotspots and mantle plumes, *Earth planet. Sci. Lett.,* **192,** 251–265.

Zucca, J.J. & Hill, D.P., 1980. Crustal Structure of the Southeast Flank of Kilauea Volcano, Hawaii, from Seismic Refraction Measurements, *Bull. seism. Soc. Am.,* **70,** 1149–1159.